

# Bi-Linear Homogeneity Enforced Calibration for Pipelined ADCs

Matthias Wagner<sup>1</sup>, Oliver Lang<sup>1</sup>, Esmaeil Kavousi Ghafi<sup>1</sup>, Andreas Schwarz<sup>2</sup> and Mario Huemer<sup>1</sup>

<sup>1</sup> Institute of Signal Processing, Johannes Kepler University, Linz, Austria

<sup>2</sup> Development Center Linz, Infineon Austria, Linz, Austria

## Abstract

Pipelined analog-to-digital converters (ADCs) are key enablers in many state-of-the-art signal processing systems with high sampling rates. In addition to high sampling rates, such systems often demand a high linearity. To meet these challenging linearity requirements, ADC calibration techniques were heavily investigated throughout the past decades.

One limitation in ADC calibration is the need for a precisely known test signal. In our previous work, we proposed the homogeneity enforced calibration (HEC) approach, which circumvents this need by consecutively feeding a test signal and a scaled version of it into the ADC. The calibration itself is performed using only the corresponding output samples, such that the test signal can remain unknown. On the downside, the HEC approach requires the option to accurately scale the test signal, impeding an on-chip implementation.

In this work, we provide a thorough analysis of the HEC approach, including the effects of an inaccurately scaled test signal. Furthermore, the bi-linear homogeneity enforced calibration (BL-HEC) approach is introduced and suggested to account for an inaccurate scaling and, therefore, to facilitate an on-chip implementation. In addition, a comprehensive stability and convergence analysis of the BL-HEC approach is carried out. Finally, we verify our concept with simulations.

## Index Terms

Adaptive Algorithm, ADC Calibration, Bi-Linear Filter, Pipelined ADC, Signal Processing

## I. INTRODUCTION

High resolution, high speed pipelined analog-to-digital converters (ADCs) are key building blocks in many of today's signal processing systems. Although the time-interleaved architecture of pipelined ADCs enables the high sampling rates, it also introduces additional error sources. Besides random errors, i.e., thermal or quantization noise, the ADC's performance is limited by systematic errors of its analog building blocks [1]. To obtain a high ADC performance, calibration techniques became an essential part of modern ADCs and were heavily investigated in recent years [2,3]. Concerning power consumption and scalability, calibration techniques are preferably carried out in the digital domain [4]. Typically, calibration consists of two parts, that are the identification of non-idealities, and their correction. On account of the identification's working principle, calibration techniques may be grouped into histogram-, correlation-, or equalization-based approaches. In general, these techniques involve either long test times [5]–[7], additional hardware components [8,9], or an exceedingly linear test signal generator (TSG) [10,11]. The latter impedes an on-chip implementation for extremely linear ADCs, as a TSG with higher linearity than the ADC is required. Therefore, much effort was devoted to relax these linearity requirements [12]. In [13], the need for an exceedingly linear TSG is omitted by injecting the test signal twice into the ADC, whereas for the second time a constant voltage offset is applied. Therewith, the TSG's nonlinearity can be identified and compensated. In literature, this is referred to as stimulus error identification and removal (SEIR) approach. Improvements of the SEIR approach, such as enhanced robustness concerning reference voltage stationarity, or a reduced hardware overhead, were investigated in [14,15], respectively. In [16], the principle of the SEIR approach is combined with a segmented nonlinearity model, which leads to a significantly reduced test time.

To analyze the SEIR-based approaches, the ADC transition function may be represented as a nonlinear function  $f(x) : \mathbb{R} \rightarrow \mathbb{R}$ . Obviously, this function violates the linearity conditions, by means that either

$$f(x + y) = f(x) + f(y) \quad \dots \text{additivity} \quad (1)$$

and/or

$$f(\alpha x) = \alpha f(x) \quad \dots \text{homogeneity} \quad (2)$$

with  $x, y$  as the system inputs and a constant  $\alpha \in \mathbb{R}$ , do not hold. For the SEIR-based approaches,  $x$  and  $y$  in (1) represent the test signal and the applied voltage offset, respectively. In this sense, they utilize the lack of additivity to identify and correct the TSG's nonlinearity.

In [17], we proposed the homogeneity enforced calibration (HEC) approach, which is based on the homogeneity condition in (2). As with the SEIR-based approaches, the test signal is injected twice into the ADC. However, for the second time, it is scaled in the analog domain by a constant factor  $\alpha$ . By shifting the focus from additivity to homogeneity, the HEC approach omits the necessity of a highly constant voltage shift. On the downside, a very precisely known scaling factor  $\alpha$  is mandatory.

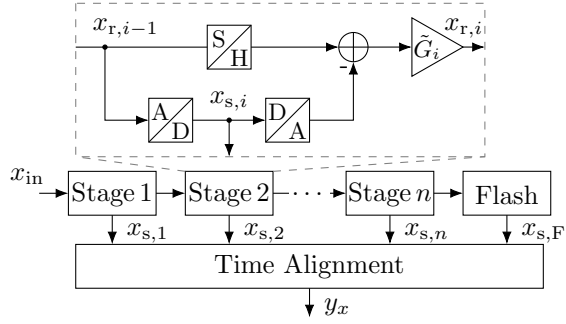


Fig. 1. Schematic of the pipelined ADC architecture including internal key building blocks of the stages [17].

The implementation of such an accurate scaling factor is a challenging task because of process, voltage, and temperature (PVT) variations. Thus, an on-chip utilization of the HEC approach is limited in real-world applications.

In this work, we propose the bi-linear homogeneity enforced calibration (BL-HEC) approach, which accounts for an inaccurate scaling factor  $\alpha$ . Note that, the BL-HEC approach maintains the fast convergence times of the original HEC approach while it restores the high spurious-free dynamic range (SFDR) improvement despite an inaccurately scaled test signal. Furthermore, the BL-HEC approach does not require any additional analog hardware components compared to its original version.

The rest of this paper is organized as follows. In Section II, the output signal of a non-ideal ADC is discussed in detail. An equivalent representation of the output signal is derived, which motivates the presented ADC post-correction model. The HEC approach is shortly reviewed in Section III, including an analysis on the impact of a scaling factor mismatch. In Section IV, two novel algorithms, which can cope with the scaling mismatch, are introduced. All findings are numerically verified in Section V, and Section VI concludes the work.

## II. SYSTEM MODEL

In this section, the basic architecture of a pipelined ADC is shortly revised. Furthermore, the interpretation of the non-ideal ADC model, introduced in [17], is extended to support the convergence analysis provided in Section V. Note that in [18], we considered an additional ADC non-ideality, i.e., nonlinear stage amplifiers. This effect is not addressed in this work for readability reasons, but can be included as discussed in [18]. Ultimately, the post-correction model employed in this work is carried out in detail.

### A. PIPELINED ADC MODEL

The main building blocks of a pipelined ADC are equally structured stages, as shown in Fig. 1. In the  $i$ th stage, the input signal  $x_{r,i-1}$  is digitized with a stage ADC, resulting in the stage output signal  $x_{s,i}$ . Note that, for the first stage  $x_{r,0} = x_{in}$ . The stage output signal is transformed back to the analog domain with a stage digital-to-analog converter (DAC) and subtracted from the stage input signal  $x_{r,i-1}$ , which is stored in a sample and hold (S&H) block. The difference signal is amplified by the stage gain  $\tilde{G}_i$  and subsequently fed into the next stage. In literature, this amplified difference signal is typically referred to as the residue signal. The last stage only comprises a flash ADC. Finally, the stage output signals  $x_{s,i}$  are used to compute the overall ADC output  $y_x$ . Due to the S&H blocks, the outputs of consecutive stages are time delayed. Thus, the time alignment in Fig. 1 is a signature building block of pipelined ADCs. By neglecting the time alignment for the sake of better readability, the overall system output may be written as

$$y_x = \sum_{i=1}^n x_{s,i} \prod_{j=1}^{i-1} \frac{1}{G_j} + x_{s,F} \prod_{j=1}^n \frac{1}{G_j}, \quad (3)$$

with  $G_j$  as the ideal stage gain and with  $x_{s,F}$  denoting the output of the final flash ADC stage. However, the ideal stage gains differ from the true stage gains  $\tilde{G}_i$  in Fig. 1 because of circuit imperfections. These differences will be referred to as gain mismatches. Additionally, the true DAC output signals do not match the ideal DAC outputs causing so-called DAC mismatches. As a result of gain and DAC mismatches, the stage outputs used in (3) are distorted and lead to a non-ideal transition function. In order to analyze the impact of these mismatches, the stage outputs are modeled as

$$x_{s,i} = x_{r,i-1} - e_{s,i}^q(x_{r,i-1}) \quad (4)$$

with  $e_{s,i}^q(x_{r,i-1})$  as the stage digitization error. The residue signal  $x_{r,i}$  may be written as

$$x_{r,i} = \tilde{G}_i (x_{r,i-1} - x_{s,i} - e_{s,i}^{DA}(x_{s,i})), \quad (5)$$

where the error  $e_{s,i}^{\text{DA}}(x_{s,i})$  represents the DAC mismatches. Inserting (4) into (5) yields the residue signal with respect to a nonideal stage gain, the stage digitization error and DAC mismatches as

$$x_{r,i} = \tilde{G}_i (e_{s,i}^q(x_{r,i-1}) - e_{s,i}^{\text{DA}}(x_{s,i})). \quad (6)$$

With (4) and (6), the overall ADC output signal of (3) may be written as

$$y_x = x_{\text{in}} - e_{s,F}^q \prod_{j=1}^n \frac{1}{G_j} + \sum_{i=1}^n \left( e_{s,i}^q \left( \frac{\tilde{G}_i}{G_i} - 1 \right) - e_{s,i}^{\text{DA}} \frac{\tilde{G}_i}{G_i} \right) \prod_{j=1}^{i-1} \frac{1}{G_j}, \quad (7)$$

where  $e_{s,F}^q$  denotes the digitization error of the final flash ADC stage. Note that, the arguments of  $e_{s,i}^q(x_{r,i-1})$  and  $e_{s,i}^{\text{DA}}(x_{s,i})$  are omitted for better readability. Introducing a relative gain error  $\zeta_i$  yields the non-ideal stage gain

$$\tilde{G}_i = G_i (1 + \zeta_i), \quad (8)$$

such that (7) may be simplified to

$$y_x = x_{\text{in}} - e_{s,F}^q \prod_{j=1}^n \frac{1}{G_j} + \sum_{i=1}^n (e_{s,i}^q \zeta_i - (1 + \zeta_i) e_{s,i}^{\text{DA}}) \prod_{j=1}^{i-1} \frac{1}{G_j}. \quad (9)$$

There, the non-ideal ADC output signal is grouped into the ideal output signal  $x_{\text{in}} - e_{s,F}^q \prod_{j=1}^n \frac{1}{G_j}$  and a summation of all stage non-idealities. This stage non-idealities are weighted by the product of preceding stage gain reciprocals. Thus, errors in the first few stages primarily affect the overall ADC nonlinearity, while errors in the last few stages may be neglected. Consequently, calibrating the most significant stages can yield sufficient calibration performances in many applications [8,19,20].

### B. POST-CORRECTION MODEL

To develop a post-correction model for the considered non-idealities, the pipelined ADC model is rearranged in the following. As shown with the summation term in (9), the non-idealities consist of the stage digitization error  $e_{s,i}^q$ , the relative gain mismatch  $\zeta_i$  and the DAC mismatches  $e_{s,i}^{\text{DA}}$ . Both, the stage digitization error as well as the DAC mismatches, are functions of the stage input, implying that different correction values are required for different input values. In order to deduce a meaningful post-correction model from the ADC model, these different correction values need to appear in the form of a parameter vector. Therefore,  $x_{s,i}$  is rewritten in vector notation as

$$x_{s,i} = \mathbf{w}_i^T \mathbf{v}_i, \quad (10)$$

with  $\mathbf{v}_i \in \mathbb{R}^{p_i}$  as a vector containing the threshold voltages of the  $i$ th stage ADC,  $p_i$  as the number of quantization levels in the  $i$ th stage, the selection subvector  $\mathbf{w}_i \in \{0, 1\}^{p_i}$  and  $(\cdot)^T$  denoting transposition. The elements of  $\mathbf{w}_i$  are

$$[\mathbf{w}_i]_j = \begin{cases} 1 & \text{if } [\mathbf{v}_i]_{j-1} < x_{r,i-1} \leq [\mathbf{v}_i]_j \\ 0 & \text{otherwise.} \end{cases}$$

where  $j = 1 \dots p_i$  and  $[\mathbf{v}_i]_0 = -\infty$ . With (4) and (10), the stage digitization error can be derived as

$$e_{s,i}^q = x_{r,i-1} - \mathbf{w}_i^T \mathbf{v}_i. \quad (11)$$

Similarly, writing the DAC mismatches in vector notation yields

$$e_{s,i}^{\text{DA}} = \mathbf{w}_i^T \mathbf{e}_i^{\text{DA}}, \quad (12)$$

with the same selection subvector  $\mathbf{w}_i$  and an error vector  $\mathbf{e}_i^{\text{DA}} \in \mathbb{R}^{p_i}$ . Finally, (9) can be written in the required form such that all errors occur in a vector. In the following, this derivation is exemplarily carried out for  $n = 2$  stages. In that case, (9) becomes

$$y_x = x_{\text{in}} - e_{s,F}^q \frac{1}{G_1 G_2} + e_{s,1}^q \zeta_1 - e_{s,1}^{\text{DA}} (1 + \zeta_1) + \frac{1}{G_1} (e_{s,2}^q \zeta_2 - e_{s,2}^{\text{DA}} (1 + \zeta_2)). \quad (13)$$

According to (6), and (11), the digitization error of the first and second stage may be written as

$$e_{s,1}^q = x_{\text{in}} - \mathbf{w}_1^T \mathbf{v}_1 \quad (14)$$

$$e_{s,2}^q = \tilde{G}_1 (x_{\text{in}} - \mathbf{w}_1^T (\mathbf{v}_1 + \mathbf{e}_1^{\text{DA}})) - \mathbf{w}_2^T \mathbf{v}_2, \quad (15)$$

respectively. With (8), (12), (14), and (15) the ADC output in (13) yields

$$y_x = x_{\text{in}} [1 + \zeta_1 + (1 + \zeta_1) \zeta_2] - e_{s,F}^q \frac{1}{G_1 G_2} - \mathbf{w}_1^T [(\zeta_1 + (1 + \zeta_1) \zeta_2) \mathbf{v}_1 + (1 + \zeta_1) (1 + \zeta_2) \mathbf{e}_1^{\text{DA}}] - \mathbf{w}_2^T \frac{1}{G_1} [\zeta_2 \mathbf{v}_2 + (1 + \zeta_2) \mathbf{e}_2^{\text{DA}}].$$

Substituting

$$\begin{aligned}\beta &= 1 + \zeta_1 + (1 + \zeta_1) \zeta_2 \in \mathbb{R}, \\ \boldsymbol{\varphi}_0 &= \begin{bmatrix} (\beta - 1) \mathbf{v}_1 + (1 + \zeta_1) (1 + \zeta_2) \mathbf{e}_1^{\text{DA}} \\ \frac{1}{G_1} (\zeta_2 \mathbf{v}_2 + (1 + \zeta_2) \mathbf{e}_2^{\text{DA}}) \end{bmatrix} \in \mathbb{R}^{p_1+p_2}, \\ \mathbf{w}_x^T &= [\mathbf{w}_1^T \quad \mathbf{w}_2^T] \in \mathbb{R}^{p_1+p_2}, \\ q_x &= e_{s,F}^q \frac{1}{G_1 G_2} \in \mathbb{R},\end{aligned}$$

in the output signal above results in

$$y_x = \beta x_{\text{in}} - \mathbf{w}_x^T \boldsymbol{\varphi}_0 + q_x, \quad (16)$$

with a scaling factor  $\beta$  and a non-ideal term  $\mathbf{w}_x^T \boldsymbol{\varphi}_0$ . The weighted digitization error of the final stage is renamed to  $q_x$ , as the overall digitization is typically referred to as quantization noise. Note that, the derivation above can easily be extended to an arbitrary number of stages. Thus, for the remainder of this work (16) is not restricted to  $n = 2$ . Analyzing (16) reveals that the considered non-idealities affect the ADC output signal in two different ways. First, an overall gain mismatch is introduced with the factor  $\beta$ , which depends on a combination of all relative gain mismatches. However, scaling does not cause any nonlinear distortion, such that it is not of particular interest in this work. Second, all remaining non-ideal effects are summarized in the vector  $\boldsymbol{\varphi}_0$ . This suggests to apply a correction term of the form  $\mathbf{w}_x^T \boldsymbol{\theta}$ , with  $\boldsymbol{\theta}$  as the calibration parameters.

The presented post-correction model may already be used for calibration. Nevertheless, as the relative gain mismatches contribute to each ADC output value weighted with the corresponding element of  $\mathbf{v}_i$ , it can be shown that the convergence times of the algorithms in the Sections III and IV are significantly improved by incorporating this information into  $\mathbf{w}_x$ . Therefore, the selection subvectors are rewritten as

$$[\tilde{\mathbf{w}}_i]_j = \begin{cases} \sum_{l=1}^i x_{s,l} \prod_{m=1}^{i-l} G_m & \text{if } j = 1 \\ [\mathbf{w}_i]_j & \text{else,} \end{cases} \quad (17)$$

where  $x_{s,l}$  introduces the required information. The subvector  $\boldsymbol{\varphi}_{0,i}$  of the parameter vector  $\boldsymbol{\varphi}_0$ , which corresponds to the  $i$ th ADC stage, transforms accordingly as

$$[\tilde{\boldsymbol{\varphi}}_{0,i}]_j = \begin{cases} \frac{1}{\sum_{l=1}^i [\mathbf{v}_l]_1 \prod_{m=1}^{i-l} G_m} [\boldsymbol{\varphi}_{0,i}]_1 & \text{if } j = 1 \\ [\boldsymbol{\varphi}_{0,i}]_j - \frac{\sum_{l=1}^i [\mathbf{v}_l]_j \prod_{m=1}^{i-l} G_m}{\sum_{l=1}^i [\mathbf{v}_l]_1 \prod_{m=1}^{i-l} G_m} [\boldsymbol{\varphi}_{0,i}]_1 & \text{else.} \end{cases}$$

The post-corrected ADC output signal with transformed non-idealities results in

$$y_x^c = \beta x_{\text{in}} + \tilde{\mathbf{w}}_x^T (\tilde{\boldsymbol{\theta}} - \tilde{\boldsymbol{\varphi}}_0) + q_x. \quad (18)$$

Choosing appropriate calibration parameters  $\tilde{\boldsymbol{\theta}}$  eliminates the non-idealities in (18), such that only the overall gain mismatch remains. If necessary, the overall gain mismatch can be removed in an additional processing step. As discussed for (9), the first few stages contribute primarily to the ADC nonlinearity. Therefore, using only these stages for calibration reduces the complexity without a severe performance degradation. As a consequence, the selection vector and the parameter vector are segmented in the subvectors  $\tilde{\mathbf{w}}_x^T = [\tilde{\mathbf{h}}_x^T \quad \mathbf{m}_x^T]$  and  $\tilde{\boldsymbol{\varphi}}_0 = [\tilde{\boldsymbol{\theta}}_0 \quad \boldsymbol{\xi}_0]$ , which correspond to covered and uncovered stages by the correction model, respectively. The covered selection subvector  $\tilde{\mathbf{h}}_x^T = [\tilde{\mathbf{h}}_1^T \quad \tilde{\mathbf{h}}_2^T \quad \dots \quad \tilde{\mathbf{h}}_q^T]$ , with  $\tilde{\mathbf{h}}_i = \tilde{\mathbf{w}}_i$ , introduces the first  $q$  stages to the post-correction model. The post-corrected output signal follows as

$$y_x^c = y_x + \tilde{\mathbf{h}}_x^T \tilde{\boldsymbol{\theta}} = \beta x_{\text{in}} + \tilde{\mathbf{h}}_x^T (\tilde{\boldsymbol{\theta}} - \tilde{\boldsymbol{\theta}}_0) - \mathbf{m}_x^T \boldsymbol{\xi}_0 + q_x. \quad (19)$$

As can be seen in the equation above,  $\tilde{\mathbf{h}}_x^T \tilde{\boldsymbol{\theta}}$  can correct for the first  $q$  stages while the less significant stages remain in the post-corrected output signal via the term  $\mathbf{m}_x^T \boldsymbol{\xi}_0$ .

As calibration requires multiple output samples, a sample index  $k$  is introduced for the corresponding variables, e.g.,  $y_x[k]$  or  $\tilde{\mathbf{h}}_x[k]$ . To identify a unique parameter vector  $\tilde{\boldsymbol{\theta}}$  for different output samples  $y_x[k]$ , the post-correction matrix  $\tilde{\mathbf{H}}_x[k]$  in

$$\begin{bmatrix} y_x^c[0] \\ y_x^c[1] \\ \vdots \\ y_x^c[k] \end{bmatrix} = \begin{bmatrix} y_x[0] \\ y_x[1] \\ \vdots \\ y_x[k] \end{bmatrix} + \underbrace{\begin{bmatrix} \tilde{\mathbf{h}}_x^T[0] \\ \tilde{\mathbf{h}}_x^T[1] \\ \vdots \\ \tilde{\mathbf{h}}_x^T[k] \end{bmatrix}}_{\tilde{\mathbf{H}}_x[k]} \tilde{\boldsymbol{\theta}} \quad (20)$$

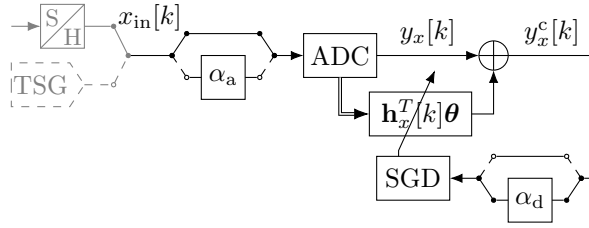


Fig. 2. Block diagram of the HEC approach including two possible signal sources, such as a TSG (dashed gray) and an arbitrary input (solid gray), e.g., the signal of the application at hand.

has to be of full rank. However, due to the interleaved architecture of pipelined ADCs, one arbitrary parameter of each stage can be represented by an offset in all parameters of the consecutive stage. Thus, the columns of  $\tilde{\mathbf{H}}_x[k]$  become linearly dependent. To remove this dependency, one arbitrary entry of each selection subvector  $\tilde{\mathbf{h}}_i$ , except in the last stage, is eliminated. In this work, always the  $p_i$ th entry is neglected. Finally, the post-corrected output signal may be written as

$$y_x^c = y_x + \mathbf{h}_x^T \boldsymbol{\theta}, \quad (21)$$

with  $\mathbf{h}_x^T = [\mathbf{h}_1^T \quad \mathbf{h}_2^T \quad \dots \quad \tilde{\mathbf{h}}_q^T]$  as the reduced selection vector and  $[\mathbf{h}_i]_j = [\tilde{\mathbf{h}}_i]_j$ , for  $j = 1 \dots p_i - 1$ . Furthermore, the new parameter vector reads as  $\boldsymbol{\theta}^T = [\boldsymbol{\theta}_1^T \quad \boldsymbol{\theta}_2^T \quad \dots \quad \boldsymbol{\theta}_q^T]$  with

$$[\boldsymbol{\theta}_i]_j = \begin{cases} [\tilde{\boldsymbol{\theta}}_1]_j & \text{if } i = 1 \\ [\tilde{\boldsymbol{\theta}}_i]_j + [\tilde{\boldsymbol{\theta}}_{i-1}]_{p_i} & \text{if } i = 2 \dots q. \end{cases} \quad (22)$$

The same parameter reduction may analogously be applied to the system model derived from (16), such that the true non-idealities  $\boldsymbol{\theta}_0$  can be represented by a modified vector  $\boldsymbol{\theta}_0$  resulting in the ADC output

$$y_x = \beta x_{\text{in}} - \mathbf{h}_x^T \boldsymbol{\theta}_0 - \mathbf{m}_x^T \boldsymbol{\xi}_0 + q_x. \quad (23)$$

### III. HOMOGENEITY ENFORCED CALIBRATION

In this section, the fundamentals of the HEC approach from [17] are briefly reviewed, followed by a detailed analysis of the performance degradation caused by the scaling factor mismatch mentioned in Section I.

#### A. HEC APPROACH FUNDAMENTALS

The HEC approach aims to enforce the homogeneity condition in (2). Therefore, an input sample  $x_{\text{in}}[k]$  is fed into the ADC twice, whereas for the second time, it is scaled with an analog scaling factor  $\alpha_a$ . As can be seen in Fig. 2, possible sources for the input signal are a TSG or an arbitrary input, e.g., the signal of the application at hand. If an arbitrary input is utilized, an additional S&H block is required. This S&H block enables injecting the same input sample twice into the ADC. The corresponding pair of output samples is denoted by  $y_x[k]$  and  $y_{\alpha_x}[k]$ , representing the ADC output of the non-scaled and scaled input, respectively. Next,  $y_x[k]$  is scaled in the digital domain with the scaling factor  $\alpha_d$  and compared with  $y_{\alpha_x}[k]$ . As a non-ideal ADC naturally violates the homogeneity condition, these two output values do not match for all possible input values. In combination with the post-correction model (21), the inequality

$$y_{\alpha_x}[k] + \mathbf{h}_{\alpha_x}^T[k] \boldsymbol{\theta} \neq \alpha_d (y_x[k] + \mathbf{h}_x^T[k] \boldsymbol{\theta}) \quad (24)$$

forms the basis of the HEC approach. Considering the difference of the two sides as the homogeneity error, the instantaneous squared homogeneity error may be written as

$$J_0[k] = (y_{\alpha_x}[k] + \mathbf{h}_{\alpha_x}^T[k] \boldsymbol{\theta} - \alpha_d (y_x[k] + \mathbf{h}_x^T[k] \boldsymbol{\theta}))^2.$$

From here on, several standard parameter identification methods [21]–[26] may be used. In our previous work, we specifically suggested an adaptive algorithm as it supports the low computational complexity of the Kaczmarz algorithm but reduces the total number of samples to be stored. A possible adaptive algorithm is the stochastic gradient descent (SGD) method [26], which results in the HEC SGD parameter update equation

$$\boldsymbol{\theta}[k] = \boldsymbol{\theta}[k-1] - \mu \Delta \mathbf{h}[k] (\Delta y[k] + \Delta \mathbf{h}^T[k] \boldsymbol{\theta}[k-1]), \quad (25)$$

with  $\Delta y[k] = y_{\alpha_x}[k] - \alpha_d y_x[k]$ ,  $\Delta \mathbf{h}[k] = \mathbf{h}_{\alpha_x}[k] - \alpha_d \mathbf{h}_x[k]$ , and  $\mu$  as the step size. In [17], it is shown that the HEC SGD approach converges in the mean towards the Wiener solution which is obtained by minimizing

$$J_\alpha^{\text{MSE}}(\boldsymbol{\theta}) = E[J_0[k]], \quad (26)$$

with  $E[\cdot]$  denoting the expectation operator. Specifically, the HEC Wiener solution reads as

$$\boldsymbol{\theta}_W = -\mathbf{R}_{hh}^{-1} \mathbf{r}_{hy}, \quad (27)$$

with  $\mathbf{R}_{hh} = E[\Delta \mathbf{h}[k] \Delta \mathbf{h}^T[k]]$  and  $\mathbf{r}_{hy} = E[\Delta \mathbf{h}[k] \Delta y[k]]$ .

Nevertheless, the main drawback of the HEC approach is that in order to obtain a good calibration performance, a perfect matching of the two scaling factors  $\alpha_a$  and  $\alpha_d$  is required. Considering PVT variations this can be challenging in a real-world on-chip implementation. In the following, the performance degradation of the HEC approach with respect to an imprecise scaling factor is carried out in detail.

### B. SCALING FACTOR MISMATCH

The effects of a scaling factor mismatch are analyzed based on the HEC Wiener solution. However, as the HEC SGD approach converges in the mean towards the HEC Wiener solution, all presented findings are also valid for the HEC SGD approach.

Using the ADC output from (23), and considering a scaling mismatch  $\alpha_d = \alpha_a - \delta$ , (27) may be written as

$$\boldsymbol{\theta}_W = \mathbf{R}_{hh}^{-1} (\mathbf{R}_{hh} \boldsymbol{\theta}_0 + \mathbf{R}_{hm} \boldsymbol{\xi}_0 - \delta E[\Delta \mathbf{h}[k] \beta x_{in}] - E[\Delta \mathbf{h}[k] (q_{\alpha_a x}[k] - (\alpha_a - \delta) q_x[k])]), \quad (28)$$

with  $\mathbf{R}_{hm} = E[\Delta \mathbf{h}[k] \Delta \mathbf{m}^T[k]]$  and  $\Delta \mathbf{m}[k] = \mathbf{m}_{\alpha_a x}[k] - (\alpha_a - \delta) \mathbf{m}_x[k]$ . Finally, assuming that  $\Delta \mathbf{h}[k]$  and the quantization noises  $q_{\alpha_a x}[k]$  and  $q_x[k]$  are uncorrelated yields

$$\boldsymbol{\theta}_W = \boldsymbol{\theta}_0 + \mathbf{R}_{hh}^{-1} \mathbf{R}_{hm} \boldsymbol{\xi}_0 - \delta \mathbf{R}_{hh}^{-1} \mathbf{r}_{hx}, \quad (29)$$

where  $\mathbf{r}_{hx} = E[\Delta \mathbf{h}[k] \beta x_{in}[k]]$ . As can be seen from the equation above, the HEC Wiener solution approximates the true ADC non-idealities if all uncovered nonidealities are neglectable and if the scaling factors match is zero, i.e.,  $\boldsymbol{\xi}_0 \approx \mathbf{0}$  and  $\delta = 0$ , respectively. However, in case of  $\delta \neq 0$ , the last term of the equation above introduces a bias according to the scaling factor mismatch. To show the performance degradation of the HEC approach with respect to the scaling factor, the SFDR improvement is considered. With a sinusoidal at the input, the SFDR represents the magnitude difference of the wanted spectral component compared to the highest unwanted spectral component caused by the ADC. As can be seen in Fig. 4 in Section V, the SFDR improvement drops to zero for small scaling factor mismatches of  $\delta = \pm 5 \cdot 10^{-3}$  considering  $\alpha_a = 0.5$ . In the following, the HEC approach is enhanced to cope with this severe performance decrease.

## IV. BI-LINEAR HEC APPROACH

As shown in [17], the HEC approach performs well in an ideal environment. However, the last section pointed out that its performance is highly sensitive to a mismatch between the analog and the digital scaling factors. To deal with this scaling factor mismatch, the fundamental inequality of the HEC approach (24) is modified by introducing a new parameter, which can compensate for the scaling factor mismatch. Specifically, the extended inequality is written as

$$y_{\alpha_a x}[k] + \mathbf{h}_{\alpha_a x}^T[k] \boldsymbol{\theta}_{NL} \neq (\alpha_d + \theta_\alpha) (y_x[k] + \mathbf{h}_x^T[k] \boldsymbol{\theta}_{NL}),$$

with  $\theta_\alpha$  as a new parameter and the renamed parameter vector  $\boldsymbol{\theta}$  as  $\boldsymbol{\theta}_{NL}$ . Computing the difference of both sides yields

$$e[k] = y_{\alpha_a x}[k] + \mathbf{h}_{\alpha_a x}^T[k] \boldsymbol{\theta}_{NL} - (\alpha_d + \theta_\alpha) (y_x[k] + \mathbf{h}_x^T[k] \boldsymbol{\theta}_{NL}). \quad (30)$$

A closer look shows that the error is no longer linear in all parameters. Caused by the newly introduced parameter  $\theta_\alpha$ , the error consists of a linear part in  $\boldsymbol{\theta}_{NL}$  and  $\theta_\alpha$ , as well as of a part that is bi-linear in  $\boldsymbol{\theta}_{NL}$  and  $\theta_\alpha$ .

In general, bi-linear models are well known in literature since they can cope with a large class of nonlinear systems while they behave, to some extent, similar as linear systems [27,28]. In [27]–[37], different methods for parameter estimation of bi-linear models are introduced, e.g., the method of least squares, the Wiener filter, a recursive least squares estimator, and a least mean squares filter. They all consider a system model, that is bi-linear in the input [27]–[32], or is purely bi-linear in the parameters [33]–[37]. In contrast to the latter, the error in (30) is linear and bi-linear in the parameters. Hence, the results derived in [33]–[37] cannot be applied in this work.

### A. BL-HEC WIENER SOLUTION

Based on the homogeneity error in (30), the mean squared error (MSE) cost function is given by

$$J_{\text{ext}}^{\text{MSE}}(\theta_\alpha, \boldsymbol{\theta}_{NL}) = E[e^2[k]]. \quad (31)$$

Note that (31) is a function of two different parameters, namely  $\theta_\alpha$  and  $\boldsymbol{\theta}_{NL}$ . As suggested in [34], the Wiener solution is derived for both parameters separately. First, (31) is minimized with respect to  $\theta_\alpha$  yielding

$$\theta_{\alpha, W} = \frac{r_{yy_\alpha}(\boldsymbol{\theta}_{NL})}{r_{yy}(\boldsymbol{\theta}_{NL})} - \alpha_d, \quad (32)$$

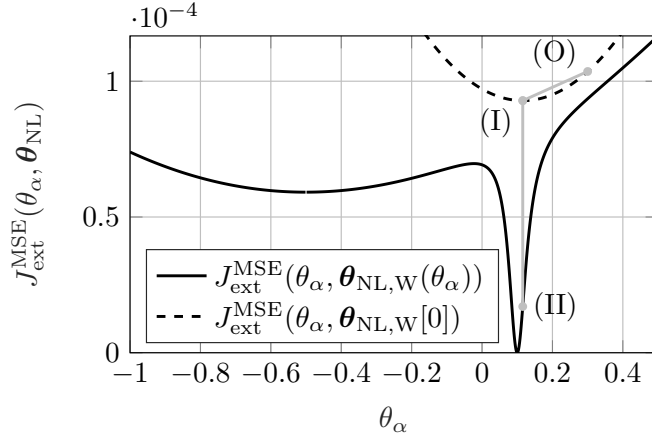


Fig. 3. Non-convex MSE cost function of an exemplary ADC.

with

$$r_{yy}(\boldsymbol{\theta}_{\text{NL}}) = E \left[ (y_x[k] + \mathbf{h}_x^T[k] \boldsymbol{\theta}_{\text{NL}})^2 \right], \quad (33)$$

$$r_{yy\alpha}(\boldsymbol{\theta}_{\text{NL}}) = E \left[ (y_{\alpha_a x}[k] + \mathbf{h}_{\alpha_a x}^T[k] \boldsymbol{\theta}_{\text{NL}}) (y_x[k] + \mathbf{h}_x^T[k] \boldsymbol{\theta}_{\text{NL}}) \right]. \quad (34)$$

It should be noted that, the Wiener solution  $\theta_{\alpha, \text{W}}$  is a function of the parameter vector  $\boldsymbol{\theta}_{\text{NL}}$  by means that each realization of  $\boldsymbol{\theta}_{\text{NL}}$  results in a different  $\theta_{\alpha, \text{W}}$ . Second, minimizing (31) with respect to  $\boldsymbol{\theta}_{\text{NL}}$  leads to

$$\boldsymbol{\theta}_{\text{NL}, \text{W}} = -\mathbf{R}_{\text{hh}}^{-1}(\theta_\alpha) \mathbf{r}_{\text{hy}}(\theta_\alpha), \quad (35)$$

with

$$\mathbf{R}_{\text{hh}}(\theta_\alpha) = E \left[ (\mathbf{h}_{\alpha_a x}[k] - (\alpha_d + \theta_\alpha) \mathbf{h}_x[k]) (\mathbf{h}_{\alpha_a x}[k] - (\alpha_d + \theta_\alpha) \mathbf{h}_x[k])^T \right] \quad (36)$$

and

$$\mathbf{r}_{\text{hy}}(\theta_\alpha) = E \left[ (\mathbf{h}_{\alpha_a x}[k] - (\alpha_d + \theta_\alpha) \mathbf{h}_x[k]) (y_{\alpha_a x}[k] - (\alpha_d + \theta_\alpha) y_x[k]) \right]. \quad (37)$$

In this case, the optimum solution is a function of the parameter  $\theta_\alpha$ . In general, a closed form solution of (32) and (35) does not exist. As in [34], the optimum solution has to be evaluated by an iterative approach, yielding the BL-HEC Wiener solution. To obtain the BL-HEC Wiener solution, the parameter vector  $\boldsymbol{\theta}_{\text{NL}, \text{W}}[0]$  is initialized as the zero vector and inserted into

$$\theta_{\alpha, \text{W}}[r] = \frac{r_{yy\alpha}(\boldsymbol{\theta}_{\text{NL}, \text{W}}[r-1])}{r_{yy}(\boldsymbol{\theta}_{\text{NL}, \text{W}}[r-1])} - \alpha_d, \quad (38)$$

with the iteration index  $r = 1 \dots R$ . In a second step, the solution of (38) is used to compute the updated parameter vector

$$\boldsymbol{\theta}_{\text{NL}, \text{W}}[r] = -\mathbf{R}_{\text{hh}}(\theta_{\alpha, \text{W}}[r])^{-1} \mathbf{r}_{\text{hy}}(\theta_{\alpha, \text{W}}[r]). \quad (39)$$

Iteratively evaluating (38) and (39) results in the iterative BL-HEC Wiener solution. Subsequently, it will be shown that this iterative procedure converges towards a minimum of (31).

At first, the MSE cost function itself is analyzed. Since the error in (30) is not linear, the cost function in (31) is not convex. To emphasize this, the cost function for one exemplary non-ideal ADC is illustrated by the solid black line in Fig. 3. To obtain this black line, (35) is inserted in (31) yielding the MSE  $J_{\text{ext}}^{\text{MSE}}(\theta_\alpha, \boldsymbol{\theta}_{\text{NL}, \text{W}}(\theta_\alpha))$  depending on  $\theta_\alpha$ . As can clearly be seen, this function is not convex and provides two distinct minima. The global minimum is located at  $\theta_\alpha \approx \delta = 0.1$  which corresponds to the scaling factor mismatch between  $\alpha_a$  and  $\alpha_d$ . A local minimum appears at  $\theta_\alpha \approx -\alpha_d = -0.5$ . A closer look on (31) shows that for  $\theta_\alpha = -\alpha_d$ , the second term vanishes, resulting in the cost function

$$J_{\text{ext}}^{\text{MSE}}(-\alpha_d, \boldsymbol{\theta}_{\text{NL}}) = E \left[ (y_{\alpha_a x}[k] + \mathbf{h}_{\alpha_a x}^T[k] \boldsymbol{\theta}_{\text{NL}})^2 \right]. \quad (40)$$

Obviously, this local minimum is of no practical interest since it simply minimizes the output of the ADC.

To show convergence of the iterative BL-HEC Wiener solution towards one of these two minima, assume a fixed  $\boldsymbol{\theta}_{\text{NL}, \text{W}}[0]$ .

Consequently, the homogeneity error (30) becomes linear in  $\theta_\alpha$ . Thus, the temporary cost function  $J_{\text{ext}}^{\text{MSE}}(\theta_\alpha, \boldsymbol{\theta}_{\text{NL,W}}[0])$  is convex with a global temporary minimum. With  $\theta_{\alpha,\text{W}}[1]$  from (38), the temporary cost function is minimized such that

$$J_{\text{ext}}^{\text{MSE}}(\theta_{\alpha,\text{W}}[0], \boldsymbol{\theta}_{\text{NL,W}}[0]) \geq J_{\text{ext}}^{\text{MSE}}(\theta_{\alpha,\text{W}}[1], \boldsymbol{\theta}_{\text{NL,W}}[0]). \quad (41)$$

Next,  $\theta_{\alpha,\text{W}}[1]$  is fixed resulting in another convex temporary cost function  $J_{\text{ext}}^{\text{MSE}}(\theta_{\alpha,\text{W}}[1], \boldsymbol{\theta}_{\text{NL,W}})$ , which is minimized by  $\boldsymbol{\theta}_{\text{NL,W}}[1]$  from (39), thus

$$J_{\text{ext}}^{\text{MSE}}(\theta_{\alpha,\text{W}}[1], \boldsymbol{\theta}_{\text{NL,W}}[0]) \geq J_{\text{ext}}^{\text{MSE}}(\theta_{\alpha,\text{W}}[1], \boldsymbol{\theta}_{\text{NL,W}}[1]). \quad (42)$$

Combining (41) and (42), one can see that each iteration of the iterative BL-HEC Wiener solution has to reduce the MSE in (31). Finally, equality in either (41) or (42) directly implies convergence of the iterative BL-HEC Wiener solution. Fig. 3 shows the temporary cost function  $J_{\text{ext}}^{\text{MSE}}(\theta_\alpha, \boldsymbol{\theta}_{\text{NL,W}}[0])$  by the dashed black line. Furthermore the discussed steps from  $J_{\text{ext}}^{\text{MSE}}(\theta_{\alpha,\text{W}}[0], \boldsymbol{\theta}_{\text{NL,W}}[0])$  to  $J_{\text{ext}}^{\text{MSE}}(\theta_{\alpha,\text{W}}[1], \boldsymbol{\theta}_{\text{NL,W}}[1])$  are marked with (O)-(II).

Nevertheless, convergence towards the global minimum strongly depends on the initialization. The proposed initialization of  $\boldsymbol{\theta}_{\text{NL,W}}[0]$  yields good convergence results. This can be immediately shown by (38) with

$$\theta_{\alpha,\text{W}}[1] = \frac{E[y_{\alpha_a x}[k]y_x[k]]}{E[(y_x[k])^2]} - \alpha_d. \quad (43)$$

Assuming sufficiently small ADC non-idealities such that  $y_{\alpha_a x}[k] \approx \alpha_a y_x[k]$ , gives  $\theta_{\alpha,\text{W}}[1] \approx \alpha_a - \alpha_d$ . Hence, already the first iteration should provide a good approximation of the global minimum.

Finally, the global minimum itself is analyzed. In general, it is not possible to state the global minimum explicitly. However, with the aid of some minor approximations, the minimum can be written in a closed form. Considering a sufficient number of stages involved in the post-correction model allows neglecting the term  $\mathbf{m}_x^T \boldsymbol{\xi}_0$  in (23), such that the post-corrected output signal may be written as

$$y_x^c \approx y_x + \mathbf{h}_x^T \boldsymbol{\theta} = \beta x_{\text{in}} + \mathbf{h}_x^T (\boldsymbol{\theta} - \boldsymbol{\theta}_0) + q_x. \quad (44)$$

Next, by substituting  $\alpha_d = \alpha_a - \delta$ , assuming  $\theta_{\alpha,\text{W}} = \delta$  and inserting (44) into (35) yields

$$\boldsymbol{\theta}_{\text{NL,W}} \approx \boldsymbol{\theta}_0 + \mathbf{R}_{\text{hh}}^{-1} E[\Delta \mathbf{h}[k] (q_{\alpha x}[k] - \alpha_a q_x[k])]. \quad (45)$$

With  $\Delta \mathbf{h}[k]$  and the quantization noises being uncorrelated,  $\boldsymbol{\theta}_{\text{NL,W}}$  approximates the true ADC non-idealities  $\boldsymbol{\theta}_0$ . Using this result and the aforementioned assumptions in (32) leads to

$$\theta_{\alpha,\text{W}} \approx \frac{E[(\alpha_a \beta x_{\text{in}}[k] + q_{\alpha x}[k]) (\beta x_{\text{in}}[k] + q_x[k])]}{E[(\beta x_{\text{in}}[k] + q_x[k])^2]} - \alpha_d.$$

Taking into account that  $E[x_{\text{in}}[k]q_x[k]] = E[x_{\text{in}}[k]q_{\alpha x}[k]] = E[q_{\alpha x}[k]q_x[k]] = 0$ , the equation above may be simplified to

$$\theta_{\alpha,\text{W}} \approx \frac{\alpha_a \beta^2}{\beta^2 + (SNR_q)^{-1}} - \alpha_d, \quad (46)$$

with  $SNR_q = E[(x_{\text{in}}[k])^2] / E[(q_x[k])^2]$  as the signal to noise ratio (SNR) regarding the quantization noise  $q_x[k]$ . In case of a full-scale input signal  $x_{\text{in}}[k]$  the maximum SNR is given as  $SNR_q \approx 6.02N + 1.76$  dB, where  $N$  is the total number of bits. The BL-HEC approach reaches its full potential for high resolution ADCs, as the term  $(SNR_q)^{-1}$  may be neglected. Consequently, (46) simplifies to  $\theta_{\alpha,\text{W}} \approx \delta$ . Thus, for a high-resolution ADC, with a sufficient number of stages covered by the post-correction model, the BL-HEC Wiener solution yields a good approximation of the true scaling factor mismatch in addition to the true ADC non-idealities. Nevertheless, it requires statistical knowledge of the output signals which might be unknown in practice. Furthermore, in (39) the matrix  $\mathbf{R}_{\text{hh}}(\theta_\alpha[r])$  needs to be inverted in each iteration step. In the next section a more computational efficient, adaptive approach is presented.

## B. BL-HEC SGD APPROACH

To derive the BL-HEC SGD approach, the homogeneity error (30) is used in the instantaneous squared error cost function as  $J_{\text{ext}}^{\text{SGD}}[k] = e^2[k]$ . The gradients of  $J_{\text{ext}}^{\text{SGD}}[k]$  with respect to  $\theta_\alpha$  and  $\boldsymbol{\theta}_{\text{NL}}$  yield the parameter updates

$$\theta_\alpha[k] = \theta_\alpha[k-1] - \mu_\alpha \left( \frac{\partial J_{\text{ext}}^{\text{SGD}}[k]}{\partial \theta_\alpha} \right) \Bigg|_{\theta_\alpha = \theta_\alpha[k-1], \boldsymbol{\theta}_{\text{NL}} = \boldsymbol{\theta}_{\text{NL}}[k-1]} \quad (47)$$

and

$$\boldsymbol{\theta}_{\text{NL}}[k] = \boldsymbol{\theta}_{\text{NL}}[k-1] - \mu_{\text{NL}} \left( \frac{\partial J_{\text{ext}}^{\text{SGD}}[k]}{\partial \boldsymbol{\theta}_{\text{NL}}} \right)^T \Bigg|_{\theta_\alpha = \theta_\alpha[k], \boldsymbol{\theta}_{\text{NL}} = \boldsymbol{\theta}_{\text{NL}}[k-1]}, \quad (48)$$

with  $\mu_\alpha$  and  $\mu_{\text{NL}}$  as the step sizes. Similar to the BL-HEC Wiener solution, both update equations depend on each other, by means they have to be evaluated alternately.

Note that in [18], it was shown that the HEC approach requires  $\sum_{i=1}^q p_i - (q-1)$  multiplications in each update step. The computational complexity of the BL-HEC SGD approach differs from the original HEC approach by the scalar valued update equation (47). As the calibrated output signals are also needed for the original HEC approach, computing (47) only adds 3 multiplications. In the next section, the convergence behavior is investigated.

### C. CONVERGENCE & STABILITY

In the following, it will be shown that the BL-HEC SGD approach converges in the mean towards its Wiener solution. Furthermore, boundaries on the step sizes  $\mu_\alpha$  and  $\mu_{\text{NL}}$  will be derived.

To show convergence, an error variable  $v_\alpha[k] = E[\theta_\alpha[k] - \theta_{\alpha,\text{W}}(\boldsymbol{\theta}_{\text{NL}}[k-1])]$ , with  $\theta_{\alpha,\text{W}}(\boldsymbol{\theta}_{\text{NL}}[k-1])$  as the Wiener solution from (32) given  $\boldsymbol{\theta}_{\text{NL}}[k-1]$ , is introduced. Subtracting  $\theta_{\alpha,\text{W}}(\boldsymbol{\theta}_{\text{NL}}[k-1])$  from both sides of (47) and computing the expected value of the result reads as

$$v_\alpha[k] = v_\alpha[k-1] + \mu_\alpha (r_{yy_\alpha}(\boldsymbol{\theta}_{\text{NL}}[k-1]) - E[(\alpha_d + \theta_\alpha[k-1]) r_{yy}(\boldsymbol{\theta}_{\text{NL}}[k-1])]). \quad (49)$$

Separating  $\alpha_d$  from (32) given  $\boldsymbol{\theta}_{\text{NL}}[k-1]$  and inserting this result into (49) yields

$$v_\alpha[k] = (1 - \mu_\alpha r_{yy}(\boldsymbol{\theta}_{\text{NL}}[k-1])) v_\alpha[k-1]. \quad (50)$$

For an appropriately chosen step size  $\mu_\alpha$ , the equation above converges in the mean towards the BL-HEC Wiener solution with respect to  $\boldsymbol{\theta}_{\text{NL}}[k-1]$ . In order to determine a practical step size without requiring any statistical knowledge, consider the posterior error

$$\acute{e}_\alpha[k] = y_{\alpha_x}[k] + \mathbf{h}_{\alpha_x}^T[k] \boldsymbol{\theta}_{\text{NL}}[k-1] - (\alpha_d + \theta_\alpha[k]) (y_x[k] + \mathbf{h}_x^T[k] \boldsymbol{\theta}_{\text{NL}}[k-1]) \quad (51)$$

and the apriori error

$$e_\alpha[k] = y_{\alpha_x}[k] + \mathbf{h}_{\alpha_x}^T[k] \boldsymbol{\theta}_{\text{NL}}[k-1] - (\alpha_d + \theta_\alpha[k-1]) (y_x[k] + \mathbf{h}_x^T[k] \boldsymbol{\theta}_{\text{NL}}[k-1]). \quad (52)$$

By inserting (47) in (51), the posterior error may be written as a function of the apriori error

$$\acute{e}_\alpha[k] = \left(1 - \mu_\alpha (y_x[k] + \mathbf{h}_x^T[k] \boldsymbol{\theta}_{\text{NL}}[k-1])\right) e_\alpha[k]. \quad (53)$$

To obtain an upper bound of the step size, the term  $(y_x[k] + \mathbf{h}_x^T[k] \boldsymbol{\theta}_{\text{NL}}[k-1])$  is approximated by the ideal ADC output. Since the maximum possible ADC output value  $y_x^{\text{max}}$  is well defined by the number bits, therefore  $2/(y_x^{\text{max}})^2$  is an approximated constant upper bound of the step size.

Stability and convergence for the parameter vector  $\boldsymbol{\theta}_{\text{NL}}$  can be shown analogously. Therefore, the error vector  $\mathbf{v}_{\text{NL}}[k] = E[\boldsymbol{\theta}_{\text{NL}}[k] - \boldsymbol{\theta}_{\text{NL},\text{W}}(\theta_\alpha[k])]$  is introduced, with  $\boldsymbol{\theta}_{\text{NL},\text{W}}(\theta_\alpha[k])$  as the solution from (35) given  $\theta_\alpha[k]$ . Subtracting  $\theta_\alpha[k]$  from both sides of (48) and computing the expected value yields

$$\mathbf{v}_{\text{NL}}[k] = \mathbf{v}_{\text{NL}}[k-1] - \mu_{\text{NL}} (\mathbf{r}_{\text{hy}}(\theta_\alpha[k]) + \mathbf{R}_{\text{hh}}(\theta_\alpha[k]) \boldsymbol{\theta}_{\text{NL}}[k-1]). \quad (54)$$

Using  $\mathbf{r}_{\text{hy}}(\theta_\alpha[k])$  from (35) allows rearranging (54) as

$$\mathbf{v}_{\text{NL}}[k] = (\mathbf{I} - \mu_{\text{NL}} \mathbf{R}_{\text{hh}}(\theta_\alpha[k])) \mathbf{v}_{\text{NL}}[k-1], \quad (55)$$

with  $\mathbf{I}$  as the identity matrix. Considering an appropriately chosen step size  $\mu_{\text{NL}}$ , the parameter vector  $\boldsymbol{\theta}_{\text{NL}}[k]$  converges in the mean towards its BL-HEC Wiener solution given the current realization  $\theta_\alpha[k]$ . Again a practical step size may be derived by utilizing the posterior error

$$\acute{e}_{\text{NL}}[k] = y_{\alpha_x}[k] + \mathbf{h}_{\alpha_x}^T[k] \boldsymbol{\theta}_{\text{NL}}[k] - (\alpha_d + \theta_\alpha[k]) (y_x[k] + \mathbf{h}_x^T[k] \boldsymbol{\theta}_{\text{NL}}[k]) \quad (56)$$

and the apriori error

$$e_{\text{NL}}[k] = y_{\alpha_x}[k] + \mathbf{h}_{\alpha_x}^T[k] \boldsymbol{\theta}_{\text{NL}}[k-1] - (\alpha_d + \theta_\alpha[k]) (y_x[k] + \mathbf{h}_x^T[k] \boldsymbol{\theta}_{\text{NL}}[k-1]). \quad (57)$$

With (48), the posterior error can be expressed as

$$\acute{e}_{\text{NL}}[k] = \left(1 - \mu_{\text{NL}} (\mathbf{h}_{\alpha_x}[k] - (\alpha_d + \theta_\alpha[k]) \mathbf{h}_x[k])^T (\mathbf{h}_{\alpha_x}[k] - (\alpha_d + \theta_\alpha[k]) \mathbf{h}_x[k])\right) e_{\text{NL}}[k]. \quad (58)$$

By neglecting  $\theta_\alpha[k]$  the step size bounds

$$0 < \mu_{\text{NL}} \leq \frac{2}{\max_k \|\Delta \mathbf{h}[k]\|_2^2} \quad (59)$$

from [17] yield a good approximation. In the following section, the analytical findings are verified by simulations.

TABLE I  
COMPARISON WITH OTHER CALIBRATION TECHNIQUES.

| Ref.             | [5]            | [7]            | [20]           | [17]           | This Work        |
|------------------|----------------|----------------|----------------|----------------|------------------|
| Samples for cal. | $1 \cdot 10^6$ | $5 \cdot 10^6$ | $5 \cdot 10^4$ | $3 \cdot 10^4$ | $4.5 \cdot 10^4$ |
| SFDR impr. (dB)  | 40.8           | 25.5           | 41             | 43             | 43.8             |
| SNDR impr. (dB)  | 34.1           | 21             | 28             | 28             | 29.5             |
| Res. (bits)      | 12             | 12             | 12             | 13             | 13               |

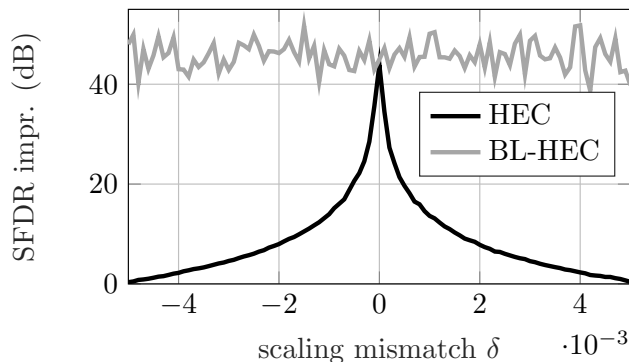


Fig. 4. SFDR improvement, considering a scaling factor mismatch  $\delta$ , of the HEC and BL-HEC approach, respectively.

## V. RESULTS

The simulation results in this section are obtained from behavioral MATLAB simulations. For that, a 13 bit pipelined ADC with six stages and a sampling rate of 100 MHz is simulated. The first five stages are modeled with 2.5 bits and ideal stage gains  $G_i = 4$ , while the final flash ADC stage includes 3 bits. The stages 1-5 incorporate gain and DAC mismatches. These mismatches were chosen from uniform probability density functions (PDFs), such that  $\zeta_i \sim \mathcal{U}[-50 \text{ LSB}, 50 \text{ LSB}]$  and  $e_{s,i}^{\text{DA}} \sim \mathcal{U}[-15 \text{ LSB}, 15 \text{ LSB}]$ . Therefore, gain and DAC mismatches in the  $i$ th stage contribute to the overall ADC nonlinearity with a maximum value of  $25/(4^{i-1})$  LSB and  $15/(4^{i-1})$  LSB, respectively. The BL-HEC approach is employed with a scaling factor  $\alpha_d = 0.5$  and a scaling factor mismatch  $\delta = 0.001$ . Furthermore, the first three stages are covered by the post-correction model. A full-scale sinusoidal at 10.77 MHz is used as the input signal and the step sizes  $\mu_{\text{NL}} = 0.5$  and  $\mu_\alpha = 0.2$  were chosen. To obtain a small steady state error,  $\mu_{\text{NL}}$  was reduced to 0.1 after  $4 \cdot 10^4$  samples. In Table I, the BL-HEC approach is compared with prior work [5,7,17,20]. As can be seen, the BL-HEC approach requires less samples for calibration, while achieving a higher SFDR improvement than [5,7,20]. The performance of the HEC approach in [17] is restored although the number of samples needed for calibration increases to  $4.5 \cdot 10^4$ . As can be seen in Fig. 4, the SFDR improvement of the HEC approach decreases significantly even for small scaling factor mismatches, whereas the BL-HEC reaches a high SFDR despite scaling mismatches. Finally, Fig. 5 shows the error norm  $\|\theta_{\text{NL}}[k] - \theta_{\text{NL,W}}\|_2$  with and without the transformed selection vector from (17). Clearly, the transformed selection vector is necessary to achieve a fast convergence.

## VI. CONCLUSION

In this work, it was shown that the performance of the HEC approach is highly sensitive to a mismatch between the analog and the digital scaling factor. To cope with this issue, the BL-HEC approach was introduced. Ultimately, simulation results of the proposed calibration technique were compared to prior work and show that the BL-HEC approach achieves a high calibration performance even for mismatching scaling factors.

## ACKNOWLEDGMENT

This work has been supported by the "LCM - K2 Center for Symbiotic Mechatronics" within the framework of the Austrian COMET - K2 program.

## REFERENCES

- [1] A. Buchwald, "High-speed time interleaved ADCs," *IEEE Communications Magazine*, vol. 54, no. 4, pp. 71–77, Apr. 2016.
- [2] K. C. Dyer, J. P. Keane, and S. H. Lewis, "Calibration and Dynamic Matching in Data Converters: Part 1: Linearity Calibration and Dynamic-Matching Techniques," *IEEE Solid-State Circuits Magazine*, vol. 10, no. 2, pp. 46–55, Jun. 2018.
- [3] K. C. Dyer, J. P. Keane, and S. H. Lewis, "Calibration and Dynamic Matching in Data Converters: Part 2: Time-Interleaved Analog-to-Digital Converters and Background-Calibration Challenges," *IEEE Solid-State Circuits Magazine*, vol. 10, no. 3, pp. 61–70, Aug. 2018.

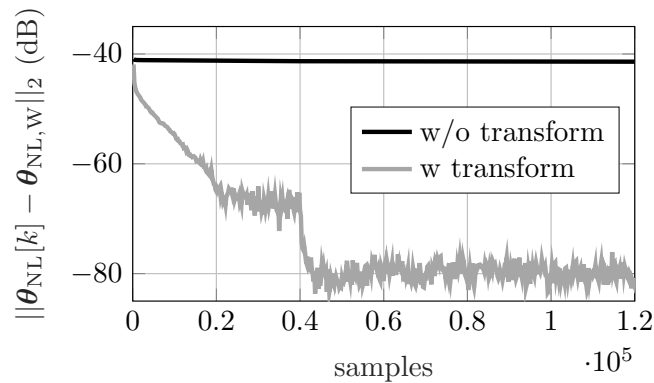


Fig. 5. Error norm with and without a transformed selection vector.

- [4] A. J. Gines, E. J. Peralias, and A. Rueda, "A survey on digital background calibration of ADCs," In Proceedings of the European Conference on Circuit Theory and Design, pp. 101–104, Antalya, Turkey, Aug. 2009.
- [5] P. Golami and M. Yavari, "Digital Background Calibration With Histogram of Decision Points in Pipelined ADCs," *IEEE Transactions on Circuits and Systems II: Express Briefs*, vol. 65, no. 1, pp. 16–20, Jan. 2018.
- [6] M.-S. Wu and H.-C. Hong, "A Digital Background Calibration Scheme for Pipelined ADCs Using Multiple-Correlation Estimation," In Proceedings of the IEEE International Symposium on Circuits and Systems, pp. 1–5, Florence, Italy, May 2018.
- [7] H. Mafi, M. Yarholi, and M. Yavari, "Statistics-Based Digital Background Calibration of Residue Amplifier Nonlinearity in Pipelined ADCs," *IEEE Transactions on Circuits and Systems I: Regular Papers*, vol. 65, no. 12, pp. 4097–4109, Dec. 2018.
- [8] N. T. Abou-El-Kheir, M. Abbas, and M. E. Khedr, "An Adaptive Digital Background Calibration Technique Using Variable Step Size LMS for Pipelined ADC," In Proceedings of the International Symposium on Communication Systems, Networks & Digital Signal Processing, pp. 835–840, Manchester, UK, Oct. 2014.
- [9] Y. Chiu, W. C. Tsang, B. Nikolić, and P. R. Gray, "Least Mean Square Adaptive Digital Background Calibration of Pipelined Analog-to-Digital Converters," *IEEE Transactions on Circuits and Systems I: Regular Papers*, vol. 51, no. 1, pp. 38–46, Jan. 2004.
- [10] Z. Yu and D. Chen, "Algorithm for dramatically improved efficiency in ADC linearity test," In Proceedings of the IEEE International Test Conference, pp. 1–10, Anaheim, CA, USA, Nov. 2012.
- [11] T. Kuyel, "Linearity testing issues of analog to digital converters," In Proceedings of the IEEE International Test Conference, pp. 747–756, Atlantic City, NJ, USA, Sep. 1999.
- [12] J. Schat, "ADC test methods using an impure stimulus: A survey," In Proceedings of the IEEE European Test Symposium, pp. 1–5, Bremen, Germany, May 2018.
- [13] Y. Jin, K. L. Parthasarathy, T. Kuyel, D. Chen, and R. L. Geiger, "Accurate testing of analog-to-digital converters using low linearity signals with stimulus error identification and removal," *IEEE Transactions on Instrumentation and Measurement*, vol. 54, no. 3, pp. 1188–1199, May 2005.
- [14] V. Varier and N. Sun, "High-Precision ADC Testing With Relaxed Reference Voltage Stationarity," *IEEE Transactions on Instrumentation and Measurement*, vol. 70, pp. 1–9, Oct. 2021.
- [15] E. Korhonen, J. Hakkinen, and J. Kostamovaara, "A Robust Algorithm to Identify the Test Stimulus in Histogram-Based A/D Converter Testing," *IEEE Transactions on Instrumentation and Measurement*, vol. 56, no. 6, pp. 2369–2374, Dec. 2007.
- [16] T. Chen, X. Jin, R. L. Geiger, and D. Chen, "USER-SMILE: Ultrafast Stimulus Error Removal and Segmented Model Identification of Linearity Errors for ADC Built-in Self-Test," *IEEE Transactions on Circuits and Systems I: Regular Papers*, vol. 65, no. 7, pp. 2059–2069, Jul. 2018.
- [17] M. Wagner, O. Lang, T. Bauernfeind, and M. Huemer, "Homogeneity Enforced Calibration of Stage Nonidealities for Pipelined ADCs," *IEEE Transactions on Circuits and Systems II: Express Briefs*, vol. 70, no. 4, pp. 1286–1290, 2023.
- [18] M. Wagner, O. Lang, E. K. Ghafi, A. Schwarz, and M. Huemer, "Homogeneity Enforced Calibration for Pipelined ADCs Including Nonlinear Stage Amplifiers," in *Conference on Ph.D Research in Microelectronics and Electronics*, pp. 153–156, 2023.
- [19] A. J. Gines, E. J. Peralias, and A. Rueda, "Black-Box Calibration for ADCs With Hard Nonlinear Errors Using a Novel INL-Based Additive Code: A Pipeline ADC Case Study," *IEEE Transactions on Circuits and Systems I: Regular Papers*, vol. 64, no. 7, pp. 1718–1729, Jul. 2017.
- [20] B. Zeinali, T. Moosazadeh, M. Yavari, and A. Rodriguez-Vazquez, "Equalization-Based Digital Background Calibration Technique for Pipelined ADCs," *IEEE Transactions on Very Large Scale Integration Systems*, vol. 22, no. 2, pp. 322–333, Feb. 2014.
- [21] S. M. Kay, *Fundamentals of Statistical Signal Processing: Estimation Theory*. Prentice Hall, 1993, vol. 1.
- [22] S. Kaczmarz, "Przybliżone rozwiązywanie układów równan liniowych. – Angenäherte Auflösung von Systemen linearer Gleichungen," *Bulletin International de l'Académie Polonaise des Sciences et des Lettres. Classe des Sciences Mathématiques et Naturelles. Série A, Sciences Mathématiques*, pp. 355–357, 1937.
- [23] M. Lunglmayr, C. Unterrieder, and M. Huemer, "Approximate least squares," In Proceedings of the IEEE International Conference on Acoustics, Speech and Signal Processing, pp. 4678–4682, Florence, Italy, May 2014.
- [24] O. Lang, "Knowledge-Aided Methods in Estimation Theory and Adaptive Filtering," Ph.D. dissertation, Johannes Kepler University, Linz, 2018.
- [25] P. S. R. Diniz et al., *Adaptive Filtering*. Springer, 2013, vol. 4.
- [26] H. Robbins and S. Monro, "A Stochastic Approximation Method," *The Annals of Mathematical Statistics*, vol. 22, no. 3, pp. 400 – 407, 1951.
- [27] R. R. Mohler and W. J. Kolodziej, "An Overview of Bilinear System Theory and Applications," *IEEE Transactions on Systems, Man, and Cybernetics*, vol. 10, no. 10, pp. 683–688, 1980.
- [28] C. Bruni, G. DiPillo, and G. Koch, "Bilinear systems: An appealing class of "nearly linear" systems in theory and applications," *IEEE Transactions on Automatic Control*, vol. 19, no. 4, pp. 334–348, 1974.
- [29] M. Li and X. Liu, "The least squares based iterative algorithms for parameter estimation of a bilinear system with autoregressive noise using the data filtering technique," *Signal Processing*, vol. 147, pp. 23–34, 2018. [Online]. Available: <https://www.sciencedirect.com/science/article/pii/S0165168418300203>
- [30] Y. Huang, J. Skoglund, and A. Luebs, "Practically efficient nonlinear acoustic echo cancellers using cascaded block RLS and FLMS adaptive filters," In Proceedings of the IEEE International Conference on Acoustics, Speech and Signal Processing, pp. 596–600, 2017.

- [31] L. Tan and J. Jiang, "Nonlinear active noise control using diagonal-channel LMS and RLS bilinear filters," In Proceedings of the IEEE International Midwest Symposium on Circuits and Systems, pp. 789–792, 2014.
- [32] H. Zhao, X. Zeng, and Z. He, "Low-Complexity Nonlinear Adaptive Filter Based on a Pipelined Bilinear Recurrent Neural Network," *IEEE Transactions on Neural Networks*, vol. 22, no. 9, pp. 1494–1507, 2011.
- [33] S. Ciochină, C. Paleologu, and J. Benesty, "Analysis of an LMS Algorithm for Bilinear Forms," In Proceedings of the International Conference on Digital Signal Processing, pp. 1–5, London, UK, Aug. 2017.
- [34] J. Benesty, C. Paleologu, and S. Ciochină, "On the Identification of Bilinear Forms With the Wiener Filter," *IEEE Signal Processing Letters*, vol. 24, no. 5, pp. 653–657, Mar. 2017.
- [35] C. Paleologu, J. Benesty, and S. Ciochină, "Adaptive filtering for the identification of bilinear forms," *Digital Signal Processing*, vol. 75, pp. 153–167, 2018. [Online]. Available: <https://www.sciencedirect.com/science/article/pii/S1051200418300228>
- [36] L. Dogariu, C. Paleologu, S. Ciochină, J. Benesty, and P. Piantanida, "Identification of Bilinear Forms with the Kalman Filter," In Proceedings of the IEEE International Conference on Acoustics, Speech and Signal Processing, pp. 4134–4138, 2018.
- [37] J. Benesty, C. Paleologu, L.-M. Dogariu, and S. Ciochină, "Identification of Linear and Bilinear Systems: A Unified Study," *Electronics*, vol. 10, no. 15, 2021. [Online]. Available: <https://www.mdpi.com/2079-9292/10/15/1790>